Eur. Phys. J. C (2012) 72:2128
DOI 10.1140/epjc/s10052-012-2128-5

THE EUROPEAN PHYSICAL JOURNAL C

Regular Article - Theoretical Physics

Glueball masses and Regge trajectories for the QCD-inspired potential

M.N. Sergeenko[a]

Institute of Physics, Belarus National Academy of Sciences, 68 Nezavisimosti Ave., Minsk 220072, Belarus

Received: 3 July 2012 / Published online: 25 August 2012

Abstract The bound state of two massive constituent gluons is studied in the potential approach. The relativistic quasi-classical wave equation with the QCD-inspired scalar potential is solved by the quasi-classical method in the complex plane. Glueball masses are calculated with the help of the universal mass formula. The hadron Regge trajectories are given by the complex non-linear function in the whole region of the invariant variable t. The Chew–Frautschi plot of the leading glueball trajectory, $\alpha_P(t)$, has the properties of a t-channel Pomeron, which is dual to the glueball states in the s channel. The imaginary part of the Pomeron is also calculated.

1 Introduction

Quantum Chromo Dynamics allows the existence of purely gluonic bound states, glueballs. These are particles whose valence degrees of freedom are gluons where the gauge field plays a more important dynamical role than in the standard hadrons. Study of glueballs is a good test of our understanding of the non-perturbative (NP) aspects of QCD, but no firm experimental discovery of such gluonic states has been obtained yet. A comprehensive review devoted to the glueballs was given in [1–3].

An important theoretical achievement in this field has been the computation of the glueball masses in lattice QCD [4]. Lattice QCD has been able to compute the low-lying glueball spectrum with a good accuracy. This predictions for glueballs are now fairly stable, at least when virtual quarks are neglected. Several candidates for the low mass glueballs with quantum numbers $J^{PC}=0^{++}$, 2^{++}, 0^{-+} and 1^{--} are under discussion. It is difficult to single out which states of the hadronic spectrum are glueballs because we lack the necessary knowledge to determine their decay properties.

Many theoretical approaches contain basic model assumptions which are difficult to prove starting from the QCD Lagrangian. Complete understanding of glueballs includes such theoretical treatments as lattice QCD, constituent models, AdS/QCD methods, and QCD sum rules [1, 3, 5]. Glueballs have been studied by using effective approach like Coulomb gauge QCD and potential model [6–12]. The potential model is very successful to describe bound states of quarks. It is also a possible approach to study glueballs [5, 9]. Recent results in the physics of glueballs with the aim set on phenomenology and the possibility of finding them in conventional hadronic experiments have been reviewed in [5].

A possible way to handle glueballs is to consider massive quasi-gluons interacting via QCD-inspired dynamics. The gluons are massless to all orders in perturbation theory, but NP effects like confinement, and their self-interactions, can be described by a constituent gluon mass. Another definition of the gluon mass was considered in [13, 14], where a realistic QCD motivated gluon propagator was obtained from approximate solution of the Dyson–Schwinger equation. The dynamical mass of gluon is defined by the position of the pole of the dressed gluon propagator.

One of open topics in hadron physics is the Pomeron. What is the Pomeron? We know the Pomeron as the highest-lying Regge (Pomeranchuk) trajectory (P trajectory) [15]. In the Regge pole theory, the leading Regge trajectories give the main contribution to the scattering amplitude. In the many high-energy reactions with small four-momentum transfer, the soft P exchange gives the dominant contribution in cross sections [16]. Next question is: what is the relation between glueballs and the Pomeron?

The relation between glueballs and the Pomeron has been investigated by many authors. Usually, the P trajectory is considered to be a linear function. However, recent small $-t$ ZEUS and H1 data for exclusive ρ and ϕ photoproduction [17–22] point out that the P trajectory is rather non-linear. The data have been explained by adding in a flavor-blind

[a] e-mail: msergeen@mail.com

hard Pomeron contribution, whose magnitude is calculated from the data for exclusive J/Ψ photoproduction [23–25]. The ZEUS, H1 as well as CDF data on $p\bar{p}$ elastic scattering data have also been analyzed by using the non-linear P trajectory [26–30].

In this work we consider two-gluon glueballs as the excited states of purely gluonic bound states of massive gluons. We accept the potential model, which is so successful in describing bound states of quarks; it is also a possible approach to study glueballs [9, 31]. To describe the two-body system we use the relativistic quasi-classical (QC) wave equation with the QCD-inspired scalar potential, in which the strong coupling is coordinate dependent, i.e., $\alpha_s = \alpha_s(r)$. We obtain two exact solutions of the relativistic QC wave equation for two components of the potential, the short-distance Coulombic term and long-distance linear one, separately. Using the interpolation procedure, we join these two solutions and obtain an interpolating mass formula, for the bound system. Using this universal mass formula, which is good to describe the mass spectra of both light and heavy quarkonia, we calculate glueball masses and reconstruct the saturating P trajectory.

This work is not a comprehensive investigation of the glueball spectroscopy. We concentrate ourself on the leading $S_z = 2$ gluonium states and take a picture where the t-channel Pomeron is dual to glueballs in the s channel. We obtain an analytic expression for the P trajectory, $\alpha_P(t)$, in the whole region of the Mandelstam invariant variable t. The trajectory is a complex non-linear function, the real part of which corresponds to the soft Pomeron in agreement with the recent HERA data and is the saturating trajectory. The imaginary component of the P trajectory is also calculated.

2 Glueballs and the Pomeron

Glueballs in full QCD are very complicated systems. Many investigations of glueball physics support the use of an effective gluon mass to describe the glueball dynamics of QCD. The lightest glueballs with positive charge conjugation $C = +$ can be successfully modeled by a two-gluon system (gluonium) in the framework of the potential approach [5].

There has been a long-standing speculation that glueballs might be the physical particles on the P trajectory [3, 5–8]. Gluonium leading states and their connection with the Pomeron have been studied in our ref. [29, 30]. We modeled glueballs to be bound states of two constituent massive gluons interacting by the Cornell potential and have shown good agreement both with the lattice calculations in the bound state region and the scattering data for the Pomeron.

2.1 Glueballs

Glueballs were suggested theoretically in [32–34] and then have been extensively studied in the framework of different approaches [3, 5, 31, 35]. These objects have not been an easy subject to study due to the lack of phenomenological support. Much debate has been associated with their properties. The main achievement of these debates is the understanding of the deep relation between the properties of the glueball states and the structure of the QCD vacuum. The basic idea is that the vacuum is filled with $J^{PC} = 0^{++}$ transverse electric glueballs which form a negative energy condensate [36].

Glueballs are bosons made only from the gluonic field; these are quarkless hadrons. They can be classed as mesons, because they are hadrons and carry zero baryon number. Glueballs must be flavor singlets, i.e., have vanishing isospin ($I = 0$) and strangeness. Like all particle states, they are specified by the quantum numbers which label representations of the Poincaré symmetry, i.e., J^{PC} and by the mass. They have the same quantum numbers as isospin 0 mesons and their decays in conventional hadrons violate the Okubo–Zweig–Iizuka rule.

Typically, every quark model meson comes in SU(3) flavor nonets—an octet and a flavor singlet. A glueball shows up as an extra (supernumerary) particle outside the nonet. In spite of such seemingly simple counting, the assignment of any given state as a glueball remains tentative even today. In a strongly coupled theory there is nothing to stop them mixing with the 'quark-based' states. These quarkless states are extremely difficult to identify in particle accelerators, because they mix with ordinary meson states. Spectrum of pure SU(3) Yang–Mills states has been extracted using computerized lattice calculations [4].

Pure gauge QCD has been investigated by lattice QCD for many years. This led to a well established glueball spectrum below 4 GeV [4]. Lattice QCD has been able to compute the low-lying glueball spectrum with a good accuracy. The data show five isoscalar resonances—$f_0(600)$, $f_0(980)$, $f_0(1370)$, $f_0(1500)$ and $f_0(1710)$. Of these the $f_0(600)$ is usually identified with the σ of chiral models. The decays and production of $f_0(1710)$ give strong evidence that it is also a quarkless meson.

At the present time, the three states 2^{++}, 0^{++}, and 0^{-+} are chosen as possible experimental glueball candidates [37, 38], because they are computed with relatively small errors in lattice calculations [39, 40]. Some experimental glueball candidates are currently known, such as $f_0(980)$, $f_0(1500)$, and $f_0(1710)$, but no definitive conclusions can be drawn concerning the nature of these states. We have got no model-independent theoretical knowledge of these hadrons. Major new experimental effort forthcoming at Jefferson Lab.

The modern development in glueball spectroscopy from various perspectives has been discussed in [1, 5, 29, 30].

All these investigations support the use of an effective gluon mass to describe the glueball dynamics of QCD. If a valence gluon is a priori massive, then it is a spin-1 particle. Such two gluons with total spin $S = 2$ in glueballs reproduce properly the lattice QCD spectrum for $C = +$ states [4] and may have five $2S + 1$ spin states: $S_z = +2, +1, 0, -1, -2$. Highest glueball trajectory with $S_z = +2$ is expected to be the Pomeron. There is work arguing that a valence gluon is a massless particle, which gains a constituent mass μ_g, either constant, or state dependent [9–14].

There are other definitions of the gluon mass [1–3], which we do not discuss here. All these arguments support the use of an effective gluon mass to describe the dynamics of QCD. It is therefore possible to envisage an approach to bound states made of constituent massive gluons. We consider here the simplest case of two-gluon glueballs, since they have always a positive conjugation charge.

2.2 The Pomeron

An open topic in hadron physics is the relation between glueballs and the Pomeron. In gauge theories with string-theoretical dual descriptions, the Pomeron emerges unambiguously. In the QCD framework the Pomeron can be understood as the exchange of at least two gluons in a color singlet state [41, 42]. The pQCD approach to the Pomeron, the Balitskiĭ–Fadin–Kuraev–Lipatov (BFKL) Pomeron, has been discussed in [43, 44]. The Pomeron can also be associated with a reggeized massive graviton [45].

The Pomeron is the vacuum exchange contribution to scattering at high energies at leading order in $1/N_c$ expansion. It is the highest-lying Regge trajectory. In the many high-energy reactions with small four-momentum transfer the P exchange gives the dominant contribution [16]. The classic soft Pomeron is constructed from multi-peripheral hadronic exchanges. It is usually believed that the soft P trajectory is a linear function,

$$\alpha_P(t) = \alpha_P(0) + \alpha'_P(0)t, \tag{1}$$

where the intercept $\alpha_P(0) = 1$ and the slope $\alpha'_P(0) = 0.25\ (\mathrm{GeV/c})^{-2}$. These fundamental parameters are very important in high-energy hadron physics. Usually, they are determined from experiment in hadron-hadron collisions.

To explain the rising hadronic cross sections at high energies, the classic soft Pomeron was replaced by a soft supercritical Pomeron with an intercept $\alpha_P(0) \simeq 1.08$. The approximate linearity (1) is true only in a small $-t$ region. The ZEUS, H1 as well as CDF data on $p\bar{p}$ elastic scattering data have also been analyzed by using the non-linear P trajectory [26]. Important theoretical results have been obtained in [46–48]. The results imply that the effective P trajectory flattens for $-t > 1\ (\mathrm{GeV/c})^2$ that is evidence for the onset of the perturbative 2-gluon Pomeron. These results may shed some light on the self-consistency of recent measurements of hard-diffractive jet production cross sections in the UA8, CDF and HERA experiments.

The issue of soft and hard Pomerons has been discussed extensively in the literature [15, 43, 44, 49, 50]. Both the IR (soft) Pomeron and the UV (BFKL) Pomeron are dealt in a unified single step. On the basis of gauge/string duality, the authors describe simultaneously both the BFKL regime and the classic Regge regime [43, 44, 49, 50]. The problem was reduced to finding the spectrum of a single j-plane Schrödinger operator. The results agreed with expectations for the BFKL Pomeron at negative t, and with the expected glueball spectrum at positive t, but provide a framework in which they are unified.

A model for the Pomeron has been put forward by Landshoff and Nachtmann where the importance of the QCD NP vacuum is evident [15]. The current data are compatible with a smooth transition from a soft to a hard Pomeron contribution which can account for the rise of σ_{tot} with s. If soft and BFKL Pomeron have a common origin, the discontinuity across the cut in the $\alpha_P(t)$ plane must have a strong t dependence which points out non-linearity of the P trajectory [51].

On the theoretical front, Tang [52, 53] used perturbative QCD (pQCD) to show that Regge trajectories are non-linear by studying high-energy elastic scattering with mesonic exchange in the case of both fixed and running coupling constants. On the experimental side, Brandt et al. [54] affirmed the existence of non-linear P trajectories from the data analysis of the UA8 and ISR experiments at CERN. They published a parametrization of P trajectories containing a quadratic term,

$$\alpha_P(t) = 1.10 + 0.25t + \alpha''_P(0)t^2, \tag{2}$$

where $\alpha''_P(0)$ is a constant, which are found from the Pomeron data fit.

Burakovsky et al. [55–57] presented a phenomenological string model for logarithmic and square root Regge trajectories. They applied a phenomenological approach based on non-linear Regge trajectories to glueball states. The parameters, i.e., intercept and threshold, or trajectory termination point beyond which no bound states should exist, were determined from Pomeron (scattering) data. They predicted masses of glueballs on the tensor trajectory. The approach was applied to available quenched lattice data and found a discrepancy between the lattice-based thresholds and the Pomeron threshold that was extracted from data.

Linear trajectories are, in fact, disfavored by various experimental data. For more details see discussions in [55–57]. The square root form of the trajectory with the parameters fitted to scattering data alone gives the same mass predictions as the fit to both the scattering data and the tensor

glueball mass, but with larger errors. Using the fit, the authors obtained the following predictions for excited glueball masses: $M(2^{++}) = 2.38 \pm 0.12$ GeV, $M(4^{++}) = 4.21 \pm 0.21$ GeV, and $M(6^{++}) = 5.41 \pm 0.28$ GeV with the same central value obtained from purely scattering Pomeron data.

The funnel-shaped Cornell potential is fixed in an extremely simple manner in terms of very small number of parameters. In pQCD, as in QED the essential interaction at small distances is instantaneous Coulombic one-gluon exchange (OGE); in QCD, it is qq, qg, or gg Coulomb scattering [51]. Therefore, one expects from OGE a Coulomb-like contribution to the potential, i.e., $V_S(r) \propto -\alpha_s/r$ at $r \to 0$.

For large distances, in order to be able to describe confinement, the potential has to rise to infinity. From lattice-gauge-theory computations [58, 59] follows that this rise is an approximately linear, i.e., $V_L(r) \simeq \sigma r$+const for large r, where $\sigma \simeq 0.15$ GeV^2 is the string tension. These two contributions by simple summation lead to the famous funnel-type (Cornell) quark–antiquark potential [58–62],

$$V(r) = V_S(r) + V_L(r) = -\frac{4}{3}\frac{\alpha_s}{r} + \sigma r; \tag{3}$$

its parameters are directly related to basic physical quantities noted above. All phenomenologically acceptable QCD-inspired potentials are only variations around this potential.

As for gluonium, the situation is very similar. The potential of gg interaction has a similar form, but different parameters. A new method called the Vacuum Correlator Model (VCM) has been used in [10–12]. In this model all NP and perturbative dynamics of quarks and gluons is universally described by lowest cumulants, i.e., gauge-invariant correlators of the type $\langle F_{\mu\nu}(x_1)\cdots F_{\lambda\sigma}(x_\nu)\rangle$. In the adjoined and fundamental representations, the final form of interaction of two massive gluons is the funnel-type potential of the form (3) [10–12]:

$$V(r) = -\frac{\alpha_a}{r} + \sigma_a r + C_0, \tag{4}$$

where $\alpha_a \equiv \alpha^{\mathrm{adj}} = 3\alpha_s^{\mathrm{fund}}$, $\sigma_a \equiv \sigma^{\mathrm{adj}} = (9/4)\sigma^{\mathrm{fund}}$; here α_s^{fund} is the light quarks strong coupling, $\sigma^{\mathrm{fund}} \equiv \sigma \simeq 0.15$ GeV^2 is the string tension. The potential (4) was used in [29, 30] to calculate glueball masses and the P trajectory.

It is hard to find an analytic solution of the wave equation for the potential (4). However, joining two exact solutions obtained separately for the short-distance Coulombic, $V_S(r)$, and long-distance linear part, $V_L(r)$, of the potential, with the help of the two-point Padé approximant we obtained the interpolating mass formula ($\hbar = c = 1$) [29, 30, 63, 64],

$$E_n^2 = 8\tilde{\sigma}\left(N + n_r + \frac{1}{2} - \tilde{\alpha}\right) + 4m^2\left(-\frac{\tilde{\alpha}^2}{N^2} + 1\right), \tag{5}$$

$$N = n_r + J + 1, \tag{6}$$

whose parameters depend on the system ($q\bar{q}$ or gg): $\tilde{\alpha} = (4/3)\alpha_s^{\mathrm{fund}}$ ($q\bar{q}$), $3\alpha_s^{\mathrm{fund}}$ (gg) and $\tilde{\sigma} = \sigma^{\mathrm{fund}}$ ($q\bar{q}$), $(9/4)\sigma^{\mathrm{fund}}$ (gg). The simple mass formula (5) describes equally well the mass spectra of all $q\bar{q}$ and $Q\bar{Q}$ mesons ranging from the $u\bar{d}$ ($d\bar{d}$, $u\bar{u}$, $s\bar{s}$) states up to the heaviest known $b\bar{b}$ systems [63, 64]. This same formula has been used to calculate the glueball masses as well [29, 30].

Regge trajectories are usually assumed to be linear in t, but there are both phenomenological and theoretical arguments supporting the idea of non-linear trajectories [55–57]. Inverting (5), we obtained the cubic equation for the angular momentum J and, therefore, the analytic dependence $J(M_n^2)$ for Regge trajectories including the P trajectory, $\alpha_P(t)$, in the whole region of the invariant variable t [29, 30, 63, 64].

The obtained "saturating" Regge trajectories were applied with success to the photoproduction of vector mesons that provide an excellent simultaneous description of the high and low $-t$ behavior of the $\gamma p \to pp$, ω, ϕ cross sections, given an appropriate choice of the relevant coupling constants (JML-model) [66–69]. As was explained in [70, 71] the hard-scattering mechanism is incorporated in an effective way by using the "saturated" Regge trajectories that are independent of t at large momentum transfers [29, 30, 63, 64].

Saturating trajectories have a close phenomenological connection to the quark–antiquark interaction which governs the mesonic structure [29, 30, 63, 64]. They provide an effective way to implement gluon exchange between the quarks forming the exchanged meson [72, 73] and lead to the asymptotic quark counting rules [74] that, model independently, determine the energy behavior of the cross section at large $-t$. This approach was successfully adopted to explain the large momentum transfer hadron-hadron interactions, as well as several photon-induced reactions [71]. The pion saturating trajectory ($\alpha_\pi^{\mathrm{sat}}(t) = -1$ when $t \to -\infty$) is in a form that reproduces the $\gamma p \to n\pi^+$ reaction around $\theta_\omega^* = 90$ [71].

A fair agreement with the experiments is achieved when saturating Regge trajectories [29, 30, 63, 64] are used for the propagators of the various exchanged mesons. This is an economical way to deal with hard-scattering mechanisms since the saturation of the Regge trajectories (approaching -1 when $-t \to \infty$) is closely related to the OGE interaction between quarks [63, 64]. The ω meson production channel is particularly instructive in this respect since pion exchange dominates the cross section [68, 69]. This same techniques and the mass formula (5) have been used in [29, 30] to reconstruct the saturating P trajectory, $\alpha_P(t)$, in the whole region of t.

In our previous calculations, the strong coupling α_s in the Cornell potential above and in the mass formula (5) is a constant value (free parameter). As we know, the strong

coupling in QCD is the function of $q^2 = t$, i.e., $\alpha_s = \alpha_s(q^2)$ is the running strong coupling. Below, we introduce the dependence $\alpha_s(r)$, and obtain similar mass formula and Regge trajectories with the use of the QCD-inspired potential.

3 The QCD-inspired potential

The strong coupling in QCD is a function of the squared four-momentum transfer, t: $\alpha_s(q^2 = t)$, or $\alpha_s(r)$ in the coordinate space. A more accurate calculation of hadronic masses and their trajectories requires the accounting for the dependence $\alpha_s(r)$ in the potential of interaction.

To find the dependence $\alpha_s(r)$, let us consider the concept of dynamically generated gluon mass, which arises from an analysis of the gluon Dyson–Schwinger (DS) equations [13, 14]. The infinite set of couple DS equations cannot be resolved analytically. One must resort to a truncation scheme. Cornwall found a gauge-invariant procedure to deal with these equations [13, 14].

An approximate resolution of the DS equations was obtained in the Feynman gauge. In Euclidean space, this solution is given by $D_{\mu\nu} = -ig_{\mu\nu}D(q^2)$, where

$$\alpha_0 D\big(q^2\big) = \frac{\alpha_s(q^2)}{q^2 + \mu^2(q^2)}, \tag{7}$$

and

$$\alpha_s\big(q^2\big) \equiv \frac{g^2(q^2)}{4\pi} = \frac{1}{b_0 \ln\{[q^2 + 4\mu^2(q^2)]/\Lambda^2\}} \tag{8}$$

with the momentum-dependent dynamical mass given by

$$\mu^2\big(q^2\big) = \mu_g^2\left[\frac{\ln[(q^2 + 4\mu_g^2)/\Lambda^2]}{\ln(4\mu_g^2/\Lambda^2)}\right]^{-\frac{12}{11}}. \tag{9}$$

Here in (7)–(9) $b_0 = (33 - 2n_f)/(12\pi)$, n_f is number of flavors, $\mu_g = \mu(0)$, Λ is the QCD dimensional parameter; typical values are $\mu_g = 500 \pm 200$ MeV and $\Lambda = 300$ MeV [13, 14].

This solution contains a dynamically generated gluon mass (9) and is another NP approach which has led to a very appealing physical picture establishing that the QCD running coupling freezes in the NP regime. Expression (8) is considered to be the QCD running coupling in momentum representation; it is frozen in the NP regime ($q^2 \to 0$),

$$\alpha_0 \equiv \alpha_s(0) = \frac{1}{2b_0 \ln(2\mu_g/\Lambda)}, \tag{10}$$

because of the presence of the dynamical gluon mass the strong effective charge, $g(q^2)$, extracted from these solutions freezes at a finite value, giving rise to an infrared fixed point for QCD [13, 14]. The gluon mass generation is a purely NP effect associated with the existence of infrared finite solutions for the gluon propagator.

Solution (7) is valid only for $\mu_g > \Lambda/2$. An important feature of the propagator (7) is that it incorporates the correct ultraviolet behavior, i.e., asymptotically obeys the renormalization group equation. This means that the gluon propagator (7) asymptotically at large q^2 takes the usual form, i.e., $D(q^2) \propto 1/q^2$, because $m^2(q^2) \to 0$ at $q^2 \to \infty$ and is valid for the entire range of momentum. The gluon is massless at the level of the fundamental QCD Lagrangian, and remains massless to all order in pQCD. The NP QCD dynamics generates an effective, momentum-dependent mass, without affecting the local SU(3)c invariance, which remains intact [13, 14].

According to Low and Nussinov the Pomeron is modeled as the exchange of two gluons [41, 42]. In [75] we modeled the P exchange by two NP gluons as suggested by Landshoff and Nachtmann [76]. We dealt with the Cornwall propagator in the context of the Landshoff–Nachtmann model and extracted the "pure" NP propagator. We have shown that the last one in combination with the multi-Pomeron asymptotic of the Quark–Gluon String Model (QGSM) [77–82], results in a good description of soft and hard distributions of secondary hadrons in a wide energy range.

Some consequences of the Cornwall solution for the gluon propagator associated to the static interaction were investigated in [83]. The OGE static potential derived from the DS equations (DS potential) was calculated numerically and compared to phenomenological potentials whose shape has been inspired by lattice computations. Application of this DS potential and comparison with some others to the description of quarkonia was considered.

The strong coupling α_s in the Cornell potential (3), (4), is a free parameter. This potential can be modified by introducing the $\alpha_s(r)$ dependence, which is unknown. However, using the mnemonic rule, $q^2 \to 1/r^2$, from (8) one can write an ansatz, for the strong running coupling in the coordinate space as follows:

$$\alpha_s(r) = \frac{1}{b_0 \ln[1/(\Lambda r)^2 + (2\mu_g/\Lambda)^2]}. \tag{11}$$

The running coupling (11) conserves the basic properties of the one (8) in the momentum representation: $\alpha_s(r \to 0) = 0$ ($q^2 \to \infty$) and $\alpha_s(r \to \infty) = \alpha_0$ ($q^2 \to 0$). We see that the running coupling (11) is frozen in the NP regime ($r \to \infty$) and is in agreement with the asymptotical freedom properties [$\alpha_s(r \to 0) \to 0$].

Thus, with the help of (11), we reach the following potential of interaction:

$$V(r) = -\frac{\tilde{\alpha}(r)}{r} + \tilde{\sigma} r, \tag{12}$$

where $\tilde{\alpha}(r) = k\alpha_s(r)$, $k = 4/3$ ($q\bar{q}$ systems) or $k = 3$ (gg system) and $\tilde{\sigma}$ as in (5). The spin-dependent corrections to

the potential (12) can also be derived from lattice QCD, but we do not consider them here.

In hadron physics, the nature of the potential is very important. There are normalizable solutions for scalarlike potentials, but not for vectorlike [84, 85]. No any problems arise and no any difficulties encountered with the numerical solution if the confining potential is purely *scalarlike*. The effective interaction has to be Lorentz-scalar in order to confine quarks and gluons [84, 85].

4 Solution of the QC wave equation

It is hard to find an analytic solution of known relativistic wave equations for the potential (12) that does not allow us to get an analytic dependence $E^2(n_r, l)$. This aim can be achieved with the use of the QC wave equation [86, 87], which for two bound particles of equal masses in the c.m. rest frame is

$$4\big[\hat{\mathbf{p}}^2 + (m_0 + V)^2\big]\tilde{\psi}(\mathbf{r}) = E^2\tilde{\psi}(\mathbf{r}), \tag{13}$$

where

$$\hat{\mathbf{p}}^2 = \left(-i\frac{\partial}{\partial r}\right)^2 + \frac{\hat{\mathbf{M}}^2}{r^2}, \tag{14}$$

$$\hat{\mathbf{M}}^2 = \left(-i\frac{\partial}{\partial \theta}\right)^2 + \frac{1}{\sin^2\theta}\left(-i\frac{\partial}{\partial \varphi}\right)^2. \tag{15}$$

Equality (13) is the second-order differential equation of the Schrödinger type in canonical form. An important feature of this equation is that, for two and more turning-point problems, it can be solved exactly by the conventional WKB method [86–89].

Appropriate solution method of the QC wave equation, which is the same for relativistic and non-relativistic systems, was developed in [87, 90]. In our method, each of the one-dimensional equations obtained after separation of the QC wave equation is solved by the same QC method. The QC wave equation (13) is separated that gives, for the potential (12),

$$\left[\frac{d^2}{dr^2} + \frac{E^2}{4} - m^2(r) - \frac{\mathbf{M}^2}{r^2}\right]\tilde{R}(r) = 0, \tag{16}$$

$$\hat{\mathbf{M}}^2\tilde{Y}(\theta,\varphi) = \mathbf{M}^2\tilde{Y}(\theta,\varphi), \tag{17}$$

where in (16) we have introduced notation,

$$m(r) = m_0 - \frac{\tilde{\alpha}(r)}{r} + \sigma r, \tag{18}$$

which can be considered as the coordinate-dependent particle mass, and m_0 is its constituent mass.

The angular QC equation (17) determines the squared angular momentum eigenvalues, $\mathbf{M}^2$, which are used in the radial equation (16). Solution of (17) has been obtained in [87–89] by the QC method in the complex plane that gives $\mathbf{M}^2 = (l + \frac{1}{2})^2$. This result means that the radial QC wave equation has always the centrifugal term $(l + \frac{1}{2})^2/r^2$ for all spherically symmetrical potentials $V(r)$. These eigenvalues for $\mathbf{M}^2$ are universal for all central potentials and not any Langer-type corrections are required [87–89].

The radial QC equation (16) has four turning points and cannot be solved analytically by standard methods. Let us use the QC method to solve the equation. The QC quantization condition appropriate to (16) in the complex plane is [29, 30, 86]

$$I = \oint_C \sqrt{\frac{E^2}{4} - m^2(r) - \frac{\mathbf{M}^2}{r^2}}\,dr = 4\pi\left(n_r + \frac{1}{2}\right). \tag{19}$$

To calculate the phase-space integral (19) in the complex plane we chose a contour C enclosing the cuts (therefore, turning points and zeros of the w.f.) at $r < 0$ and $r > 0$ between the turning points r_1, r_2 and r_3, r_4, respectively. Outside the contour C, the problem has two singularities, i.e. at $r = 0$ and ∞. Using the standard method of stereographic projection, we should exclude the singularities outside the contour C. Excluding these infinities we have, for the integral (19), $I = I_0 + I_\infty$, where $I_0 = -2\pi(l + \frac{1}{2})$ is contribution of the centrifugal term. The integral I_∞ is calculated with the help of the replacement of variable, i.e., $z = 1/r$, which gives $I_\infty = 2\pi(E^2/8\sigma + \tilde{\alpha}_0)$, where $\tilde{\alpha}_0 = k\alpha_0$ and α_0 is the strong coupling in the NP regime (10). Here we took into account the asymptotic properties of the running coupling (11) and its derivative: $\alpha_s(r) = 0$, $\alpha_s'(r) = 0$ at $r \to 0$. The calculations result in the squared total energy eigenvalues,

$$E_n^2 = 8\tilde{\sigma}(2n_r + J + 3/2 - \tilde{\alpha}_0). \tag{20}$$

Putting in (20) $\tilde{\alpha}_0 = 0$ we come to well known result for the linear potential, $E_n^2 = 8\tilde{\sigma}(2n_r + J + 3/2)$.

This QC method reproduces the exact energy eigenvalues for all known solvable problems in quantum mechanics [87]. In our QC method not only the total energy, but also momentum of a particle-wave in bound state is the *constant of motion*. Solution of the QC wave equation in the whole region is written in elementary functions as [90],

$$\tilde{R}(r) = C_n \begin{cases} \frac{1}{\sqrt{2}}\exp(|p_n|r - \phi_1), & r < r_1, \\ \cos(|p_n|r - \phi_1 - \frac{\pi}{4}), & r_1 \le r \le r_2, \\ \frac{(-1)^n}{\sqrt{2}}\exp(-|p_n|r + \phi_2), & r > r_2, \end{cases} \tag{21}$$

where $C_n = \sqrt{2|p_n|/[\pi(n + \frac{1}{2}) + 1]}$ is the normalization coefficient, p_n is the corresponding eigenmomentum, $\phi_1 = -\pi(n + \frac{1}{2})/2$ and $\phi_2 = \pi(n + \frac{1}{2})/2$ are the values of the

phase-space integral at the turning points x_1 and x_2, respectively. In the classically allowed region $[x_1, x_2]$, the solution is

$$\tilde{R}_{nl}(r) = C_n \cos\left(|p_n| r + \frac{\pi}{2} n\right), \tag{22}$$

i.e., has the form of a standing wave. This solution is appropriate for two-turning-point problems both in non-relativistic and relativistic cases with the corresponding eigenmomenta p_n.

For example, in case of the non-relativistic Coulomb problem, the total energy eigenvalues have the form of kinetic energy of a free particle [87, 90],

$$E_n = \frac{p_n^2}{2m}, \quad p_n = \frac{i\alpha m}{n_r + l + 1}, \tag{23}$$

where $p_n = m v_n$ is the non-relativistic momentum eigenvalue with the imaginary discrete velocity, $v_n = i\alpha/(n_r + l + 1)$. This means, for example, that the motion of the electron in a hydrogen atom is free, but restricted by the "walls" of the potential. This is *free finite motion* of a particle-wave in bound state. One should note that the QC eigenfunctions (22) correspond to the asymptote of the exact solution of the Schrödinger equation, i.e., the principal term of the asymptotic series of the corresponding exact solution [90].

It is an experimental fact that the dependence E_n^2 is linear for light mesons. However, at present, the best way to reproduce the experimental masses of light hadrons is to rescale the entire mass spectrum assuming that the masses M_n of the mesons are expressed by the relation [91]

$$E_n^2 = M_n^2 - C^2, \tag{24}$$

where C is a constant energy (free parameter). Relation (24) is used to shift the spectra and appears as a means to simulate the effects of unknown structure approximately. This constant can be interpreted as a renormalization of the vacuum energy [92]. It has been suggested that the confinement potential has a complex Lorentz structure, and the relation (24) used to shift the spectra appears as a means to simulate approximately the effects of this structure. This constant can be connected with the structure of the QCD vacuum, filled with $J^{PC} = 0^{++}$ transverse electric glueballs which form a negative energy condensate [36].

The oscillator-type expression (20) does not require any additional free parameter. It contains the needed shift in the form of the interference term $-8\tilde{\alpha}_0\tilde{\sigma}$ of the Coulombic and linear terms of the potential (12). Formula (20) is good to describe spectra of light hadrons, but not heavy quarkonia.

The asymptotic expression (20) is defined by the singularities at $r = 0$ and $r \to \infty$. The leading singularity in the phase-space integral (19) at $r \to \infty$ is given by the quadratic term $(\sigma r)^2$ originating from the linear part of the potential (12), which gives the dominant contribution in (19) at infinity. But the term $\propto r^2$ suppresses a very important contribution of the Coulombic interaction at small and moderate distances r.

It is known that heavy $Q\bar{Q}$ systems can be treated non-relativistically and, for low states of heavy quarkonia, the main contribution to the boundary energy comes from OGE term of the potential (12), i.e., in the first approximation one can neglect the confining linear term. A reliable consideration of the excited $Q\bar{Q}$ states requires a completely relativistic treatment.

Let us consider the radial equation (16) just for the Coulombic part $V_S(r)$ of the potential (12). The QC quantization condition in the complex plane is

$$\oint_C \sqrt{\frac{E^2}{4} - \left[m - \frac{\tilde{\alpha}(r)}{r}\right]^2 - \frac{\mathbf{M}^2}{r^2}}\, dr = 2\pi\left(n_r + \frac{1}{2}\right), \tag{25}$$

and the integral is calculated analogously to the above case. A contour C encloses the classical turning points r_1 and r_2 and cut between them. Using the same solution method of stereographic projection, we obtain, for the integral (25) outside the contour C at $r = 0$ and ∞: $I = I_0 + I_\infty$, where $I_0 = -2\pi(l + \frac{1}{2})$ and $I_\infty = 2\pi(\tilde{\alpha}_0 m/\sqrt{-E^2/4 + m^2})$. This gives

$$E_n^2 = 4m^2\left[-\frac{\tilde{\alpha}_0^2}{(n_r + l + 1)^2} + 1\right]. \tag{26}$$

Again, here we took into account the asymptotic properties of the strong running coupling (11) at $r \to 0$ and $r \to \infty$.

Thus, we have two exact analytic expressions (20) and (26) for two asymptotic components of the potential (12) (Coulombic and linear). Now, we can use the same approach as in [29, 30, 63, 64], i.e., derive the interpolating mass formula for E_n^2, which satisfies both of the above constraints: the exact energy eigenvalues (20) and (26). To derive such a formula we use the two-point Padé approximant [93],

$$[K/N]_{\mathrm{f}}(z) = \frac{\sum_{i=0}^{K} a_i z^i}{\sum_{j=0}^{N} b_j z^j}, \tag{27}$$

with $K = 3$ and $N = 2$. We take $K = 3$ and $N = 2$ because this is a simplest choice to satisfy the two asymptotic limits (20) and (26). Simple calculations give the following interpolating mass formula:

$$E_n^2 = 4m^2\left[\frac{2\tilde{\sigma}}{m^2}\left(N + n_r + \frac{1}{2} - \tilde{\alpha}_0\right) - \frac{\tilde{\alpha}_0^2}{N^2} + 1\right], \tag{28}$$

where N is the principal quantum number (6). Note that the two exact asymptotic expressions (20) and (26) for E_n^2 have the form of the squared total energy for two free relativistic particles, i.e., $E_n^2 = 4(p_n^2 + m^2)$.

The mass formula (28) is similar to one (5) but differs by the sense of the strong coupling $\tilde{\alpha}_0$. This quantity is given by the asymptotic value (10) which depends on the physical values μ_g and Λ. The universal mass formula (28) is good to describe the mass spectra of both light and heavy quarkonia. To demonstrate its efficiency we calculate the leading state masses of ρ and ϕ families (see Tables 1, 2, where masses are in MeV).

In this calculations the frozen strong coupling (10) depends on the ratio μ_g/Λ. From the fit results we found the optimal value for the constituent gluon mass, $\mu_g = 416$ MeV. The QCD dimensional parameter Λ as others is found from the best fit to the available particle data [94]. For light quarks, we take the average effective mass, $m_n = (m_u + m_d)/2$ MeV. The best fit to the data is achieved for $m_n = 144$ MeV.

The mass formula (28) is appropriate to calculate the glueball masses as well. In this case we use the potential (12) with the parameters of gg interaction. Calculation results for the gluonium leading state masses are shown in Table 3.

Table 1 The ρ-family $J = l + 1$ leading states

Meson	J^{PC}	$E_n^{\rm ex}$	$E_n^{\rm th}$	Parameters in (28)
$\rho\ (1S)$	1^{--}	775	775	$\Lambda = 487$ MeV
$a_2\ (1P)$	2^{++}	1318	1319	$\sigma = 0.137$ GeV^2
$\rho_3\ (1D)$	3^{--}	1689	1689	$m_n = 144$ MeV
$a_4\ (1F)$	4^{++}	2001	1989	
$\rho\ (1G)$	5^{--}		2249	
$\rho\ (1H)$	6^{++}		2481	
$\rho\ (2S)$	1^{--}	1720	1683	
$\rho\ (2P)$	2^{++}		1986	
$\rho\ (2D)$	3^{--}		2247	
$\rho\ (2F)$	4^{++}		2480	
$\rho\ (3S)$	1^{--}		2245	

Table 2 The ϕ-family $J = l + 1$ leading states

Meson	J^{PC}	$E_n^{\rm ex}$	$E_n^{\rm th}$	Parameters in (28)
$\phi\ (1S)$	1^{--}	1020	1019	$\Lambda = 445$ MeV
$f_2\ (1P)$	2^{++}	1525	1525	$\sigma = 0.125$ GeV^2
$\phi_3\ (1D)$	3^{--}	1854	1854	$m_{\rm s} = 414$ MeV
$f_4\ (1F)$	4^{++}	2018	2119	
$\phi\ (1G)$	5^{--}		2349	
$\phi\ (1H)$	6^{++}		2556	
$\phi\ (2S)$	1^{--}	1820	1820	
$\phi\ (2P)$	2^{++}	2011	2103	
$\phi\ (2D)$	3^{--}		2340	
$\phi\ (2F)$	4^{++}		2551	
$\phi\ (3S)$	1^{--}		2327	

Equation (28) is an ansatz (as the potential (12)), which is based on two exact asymptotic expressions (20) and (26). It allows us to get an *analytic* expression for Regge trajectories in the whole region. Transform (28) into the cubic equation for the angular momentum $J(t = E^2)$,

$$J^3 + a_1(t)J^2 + a_2(t)J + a_3(t) = 0, \tag{29}$$

where $a_1(t) = \lambda(t) + 2\tilde{n}$, $a_2(t) = 2\tilde{n}\lambda(t) + \tilde{n}^2$, $a_3(t) = \tilde{n}^2\lambda(t) - \tilde{\alpha}^2 m^2/(2\tilde{\sigma})$, $\tilde{n} = n_r + 1$, $\lambda(t) = (-t + 4m^2)/(8\tilde{\sigma}) + 2n_r + 3/2 - \tilde{\alpha}$. Equation (29) has three (complex in general case) roots: $J_1(t)$, $J_2(t)$, and $J_3(t)$. The real part of the first root, $\mathrm{Re}\, J_1(t)$ (Chew–Frautschi plot), gives the analytic expression for Regge trajectories,

$$\mathrm{Re}\,\alpha(t) = \begin{cases} 2\sqrt{-p}\cos(\phi/3) - a_1/3, & Q < 0; \\ -a_1/3\ (q = 0), & Q = 0; \\ f_1 + f_2 - a_1/3, & Q > 0, \end{cases} \tag{30}$$

where $\phi(t) = \arccos(-q/\sqrt{-p^3})$, $p(t) = -a_1^2/9 + a_2/3$, $q(t) = a_1^3/27 - a_1 a_2/6 + a_3/2$, $Q(t) = p^3 + q^2$, $f_1(t) = (-q + \sqrt{Q})^{1/3}$, $f_2(t) = (-q - \sqrt{Q})^{1/3}$. Expression (30) supports the existing experimental data and gives the saturating Regge trajectories including the Pomeron in the whole region of t.

The imaginary part of the complex Regge trajectories is given by the expression

$$\mathrm{Im}\,\alpha(t) = \sqrt{3}(f_1 - f_2)/2, \qquad Q > 0. \tag{31}$$

The threshold (trajectory termination point), beyond which no bound states should exist, is defined from the equation, $Q(t) = p^3 + q^2 = 0$ (see notations above).

The Chew–Frautschi plots of the complex Regge trajectories are shown in Figs. 1, 2 and 3. The general property of all trajectories given by (30) is that they saturate, i.e., $\mathrm{Re}\,\alpha(t) \to -1$ at $-t \to \infty$. The P trajectory corresponds to the soft supercritical Pomeron and is in agreement with the HERA data at small $-t$ [17–22]. Our P trajectory and

Table 3 Glueball $J = l + 2$ leading states

Glueball	J^{PC}	$E_n^{\rm ex}$	$E_n^{\rm th}$	Parameters in (28)
$f_0\ (1710)$	2^{++}	1710	1710	$\Lambda = 321$ MeV
$f_0\ (1P)$	3^{--}		2405	$\sigma_a = 0.329$ GeV^2
$f_0\ (1D)$	4^{++}		2921	$\mu_g = 416$ MeV
$f_0\ (1F)$	5^{--}		3350	
$f_0\ (2S)$	2^{++}		2898	
$f_0\ (2P)$	3^{--}		3338	
$f_0\ (2D)$	4^{++}		3720	
$f_0\ (3S)$	2^{++}		3711	
$f_0\ (3P)$	3^{--}		4057	
$f_0\ (3D)$	4^{++}		4374	

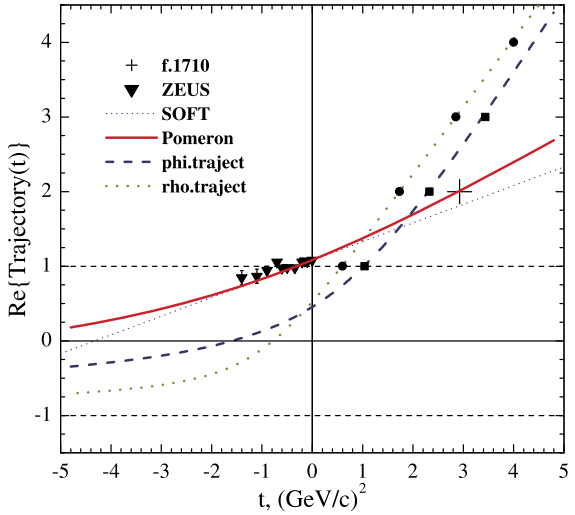

Fig. 1 The Chew–Frautschi plots of the leading ρ, ϕ and P complex Regge trajectories calculated with the use (30). Parameters are found from the fit of combined HERA ρ and ϕ data (*triangles*) [17–22], and 2^{++} glueball candidate $f_0(1710)$ (*cross*) [65]. *Solid curve* is the P trajectory, *dotted* and *dashed lines* show the leading ρ and ϕ saturating Regge trajectories

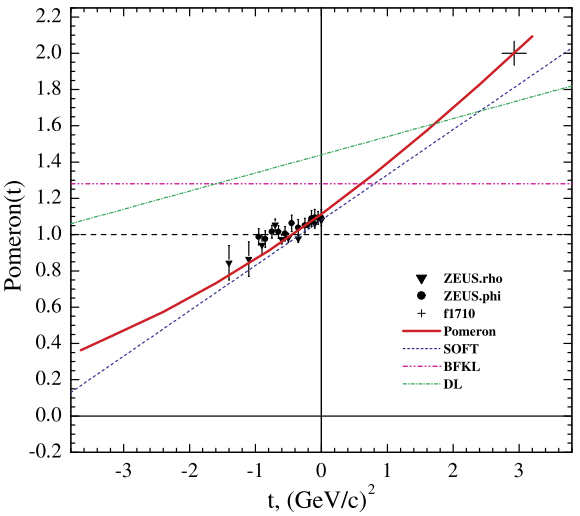

Fig. 2 The vacuum effective $J = l + 2$ Regge trajectory. *Solid curve* is the P trajectory obtained from (30) with the parameters found from the fit to combined HERA ρ (*triangles*) and ϕ (*circles*) data [17–22], and 2^{++} glueball candidate $f_0(1710)$ (*cross*) [65]. Other lines show the classic "soft", BFKL, and Donnachie–Landshoff "hard" Pomerons

its comparison with the known other Pomerons are shown in Fig. 2.

The effective P trajectory has similar properties as all quark–antiquark trajectories given by (30). It is asymptotically linear at $t \to \infty$ with the slope $\alpha'_P = 1/(8\sigma_a) \simeq 0.380\ (\mathrm{GeV/c})^{-2}$, and flattens off at -1 for $-t \to \infty$. As all Regge trajectories the P trajectory is the monotonically rising function at the interval $(-\infty, \infty)$.

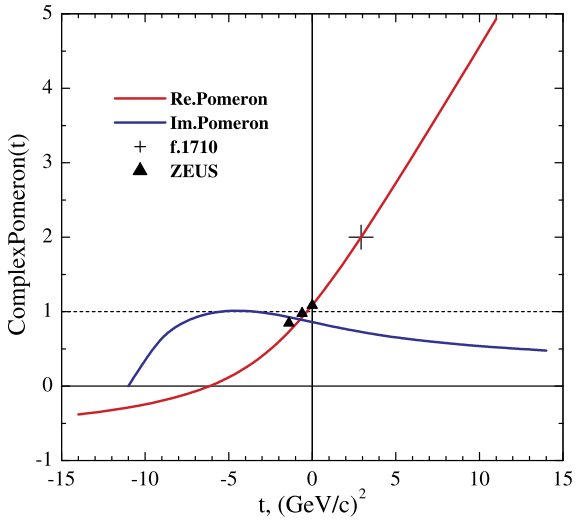

Fig. 3 The real and imaginary components of the gluonium $J = l + 2$ complex Regge trajectory (the Pomeron). *Triangles* show combined HERA ρ and ϕ data [17–22]

Parameters of the function $\mathrm{Re}\,\alpha_P(t)$ are found from the best fit to the combined ZEUS ρ (triangles) and ϕ (circles) scattering data [17], and glueball candidate $f_0(1710)$ [65] (cross) with quantum numbers $J^{PC} = 2^{++}$ ($l = 0$, $S_z = +2$) in bound state region. The intercept and slope of the P trajectory at $t = 0$ are

$$\alpha'_P(0) = 1.083, \qquad \alpha'_P(0) = 0.280\ (\mathrm{GeV/c})^2. \tag{32}$$

The hard BFKL Pomeron has intercept $\alpha_P(0) \simeq 1.43$ [43, 44]. The Pomeron with such properties results in too fast growth of the total cross sections.

Recent studies of exclusive electro-production of vector mesons at JLab [66, 67] made it possible for the first time to play with two independent hard scales: the virtuality Q^2 of the photon, which sets the observation scale, and the momentum transfer t to the hadronic system, which sets the interaction scale. They reinforce the description of hard-scattering processes in terms of few effective degrees of freedom relevant to the Jlab-Hermes energy range [72].

The study of exclusive electro-production of ω mesons, completed at JLab [66, 67], provides us with an original insight on the space time structure of hard-scattering processes between the constituents of hadrons. It was shown that the higher order mechanisms are more economically described in terms of a few effective degrees of freedom: dressed parton propagators, saturating Regge trajectories and electromagnetic form factors of off-shell meson. The success of this description in several channels is a strong hint that they are the relevant degrees of freedom in the JLab-Hermes energy range. In addition, they provide us with a link with more fundamental approaches of NP QCD: *ab initio* lattice-gauge calculations or potential models.

The two-Pomeron picture (soft plus BFKL Pomeron) gives a very good fit to the total cross section for elastic J/Ψ photoproduction and the charm structure function F_2^c over the whole range of $Q^2 = -t$ [95]. The hard BFKL Pomeron has the intercept $\alpha_{\mathrm{BFKL}}(0) \simeq 1.43$. Next-to-leading order estimates give, for the BFKL intercept values 1.26 to 1.30, which is closer to the soft supercritical Pomeron. However, the results of the experiments and the found higher order corrections make it quite unclear what the BFKL Pomeron is. Another question is: what is the intercept of the BFKL Pomeron, if the pQCD is non-applicable in this scale, i.e., at $t = 0$? On the other hand, the saturated P trajectory (30) has the properties of the soft supercritical Pomeron at small $-t$ and saturates at large $-t$ according to the pQCD prediction.

5 Conclusion

We have considered glueballs as bound states of constituent massive gluons and investigated their properties in the framework of the potential approach. The constituent gluon picture could be questioned since potential models have serious difficulties in reproducing all the currently known lattice QCD data. In spite of non-relativistic phenomenological nature, the potential approach can be used to describe glueballs. Fair description of quarkonium states give us a confidence that we are on the right way to describe glueballs.

The physical properties of constituent gluons are still a matter of controversy. Within the framework of potential models, gluons are supposed to be massless or massive, i.e., with either a helicity-1 or a spin-1 particles. We have dealt with the simplest two-gluon glueballs, but mass and spin in different works are very different. If valence gluons are assumed to be helicity-1 particles, then their spin has only two projections: $S_z = \pm 1$. In this work gluons are considered as massive spin-1 particles with projections $S_z = -1, 0, +1$. The properties of these pure glue states are not completely understood.

We have analyzed two exact asymptotic solutions of relativistic QC wave equation for the QCD-inspired scalar potential with the coordinate-dependent strong coupling, $\alpha_s(r)$. One needs to stress that the behavior of the potential and exact form of the coupling $\alpha_s(r)$ are not so important in the intermediate region: in fact, the results depend on the asymptotic behavior of the potential at $r \to 0$ and $r \to \infty$. Our QC method in the complex plane to resolve the eigenvalue problem is rather simple and allows to get the analytic result. Using two asymptotes, corresponding to the short-distance Coulombic and long-distance linear components of the potential, we have derived the universal mass formula (28) and calculated the glueball masses, which are in agreement with the lattice data.

We have considered glueballs as the physical particles on the P trajectory. To reproduce the trajectory, we have inverted the mass formula (28) and derived the analytic expression (30) for the P trajectory, $\mathrm{Re}\,\alpha_P(t)$, and its imaginary part $\mathrm{Im}\,\alpha_P(t)$ in the whole region of t. In the scattering region, at $-t \gg \Lambda_{\mathrm{QCD}}$, the trajectory flattens off at -1, i.e., it has asymptote $\alpha_P(t \to -\infty) = -1$ (saturates). In the bound state region, at large timelike t, the P trajectory is linear in accordance with the string model.

It is known that the fixed-number of particles with a potential description cannot be used for strict relativistic description. Strict description of the Pomeron presupposes multiparticle description of the system. For perturbative regime with the Pomeron scattering, the dominant contribution comes from the BFKL Pomeron. However, experimental data and our simple calculations in the framework of the potential approach support the conception of the soft supercritical Pomeron as observed at the presently available energies. The saturating Regge trajectories (30) obtained in this work effectively include short- and long-distance dynamics of constituents.

In this paper we have not considered helicities and spin properties of gluons. This topic has been discussed in detail elsewhere [5]. The existing data and simple analysis performed in this work confirm the existence of the Pomeron which is a complex non-linear function with the properties of soft supercritical Pomeron at small $-t$ and saturates at large squared momentum transfers.

Acknowledgements I would like to thank N.M. Shumeiko, A.A. Pankov and Yu.A. Kurochkin for support and constant interest in this work.

References

1. V. Mathieu, N. Kochelev, V. Vento, Int. J. Mod. Phys. E **18**, 1 (2009). arXiv:0810.4453v1
2. N. Boulanger, F. Buisseret, V. Mathieu, C. Semay, Eur. Phys. J. A **38**, 317 (2008)
3. E. Klempt, A. Zaitsev, Phys. Rep. **454**, 1 (2007)
4. Y. Chen et al., Phys. Rev. D **73**, 014516 (2006)
5. V. Mathieu, F. Buisseret, C. Semay, Phys. Rev. D **77**, 114022 (2008). arXiv:0802.0088
6. V. Mathieu, C. Semay, B. Silvestre-Brac, Phys. Rev. D **77**, 094009 (2008). arXiv:0803.0815
7. V. Mathieu, C. Semay, B. Silvestre-Brac, Phys. Rev. D **74**, 054002 (2006). arXiv:hep-ph/0605205
8. V. Mathieu, C. Semay, B. Silvestre-Brac, Phys. Rev. D **77**, 094009 (2008). arXiv:0810.4453v1
9. F. Brau, C. Semay, Phys. Rev. D **72**, 078501 (2005)
10. A.B. Kaidalov, Yu.A. Simonov, Phys. Lett. B **636**, 101 (2006). arXiv:hep-ph/0512151
11. Yu.A. Simonov, Nucl. Phys. B **324**, 67 (1989)
12. H.G. Dosch, Yu.A. Simonov, Z. Phys. C **45**, 147 (1989)
13. J.M. Cornwall, Phys. Rev. D **26**, 1453 (1982)
14. A.C. Aguilar, J. Papavassiliou, J. High Energy Phys. **0612**, 012 (2006)

15. A. Donnachie, H.G. Dosch, P.V. Landshoff, O. Nachtmann, *Pomeron Physics and QCD* (Cambridge University Press, Cambridge, 2002)
16. P.V. Landshoff, in *The Total Cross-Section at the LHC*. Lectures at School on QCD, Calabria, July 2007. arXiv:0709.0395
17. J. Breitweg et al. (ZEUS Collaboration), Eur. Phys. J. C **1**, 81 (1998)
18. D. Aston et al., Nucl. Phys. B **209**, 56 (1982)
19. M. Derrick et al. (ZEUS Collaboration), Phys. Lett. B **293**, 465 (1992)
20. M. Derrick et al. (ZEUS Collaboration), DEZY 94-117 (1994)
21. T. Ahmed et al. (H1 Collaboration), Phys. Lett. B **299**, 374 (1993)
22. T. Ahmed et al. (H1 Collaboration), DEZY 94-133 (1994)
23. A. Donnachie, P.V. Landshoff, Phys. Lett. B **518**, 63 (2001)
24. A. Donnachie, P.V. Landshoff, Phys. Lett. B **470**, 243 (1999)
25. A. Donnachie, P.V. Landshoff, M/C-TH 99-16, DAMTP-1999-167
26. R. Fiore, L.L. Jenkovszky, F. Paccanoni, A. Prokudin, Phys. Rev. D **68**, 014005 (2003)
27. A.A. Godizov, Phys. Rev. D **78**, 034028 (2008). arXiv:0710.1793
28. A.A. Godizov, V.A. Petrov, J. High Energy Phys. **0707**, 083 (2007). arXiv:hep-th/0701121
29. M.N. Sergeenko, Europhys. Lett. **89**, 11001 (2010). arXiv:1107.1671v1. A Letter of Journal Exploring the Frontiers of Physics, EPL, Best of 2010, ISSN 0295-5075, p. 9
30. M.N. Sergeenko, Rep. Belarus Natl. Acad. Sci. **55**(5), 40 (2011)
31. W.S. Hou, C.S. Luo, G.G. Wong, Phys. Rev. D **64**, 014028 (2001)
32. H. Fritzsch, P. Minkowsky, Nuovo Cimento A **30**, 393 (1975)
33. J.F. Bolzan et al., Phys. Rev. Lett. **35**, 419 (1975)
34. P.G.O. Freund, Y. Nambu, Phys. Rev. Lett. **37**, 1646 (1975)
35. B. Diekman, Phys. Rep. **159**, 99 (1988)
36. J.F. Donoghue, K. Johnson, B.A. Li, Phys. Lett. B **99**, 416 (1981)
37. B.S. Zou, Nucl. Phys. A **655**, 41 (1999)
38. D.V. Bugg, M.J. Peardon, B.S. Zou, Phys. Lett. B **486**, 49 (2000). arXiv:hep-ph/0006179
39. C.J. Morningstar, M.J. Peardon, Phys. Rev. D **60**, 034509 (1999). arXiv:hep-lat/9901004
40. Y. Chen et al., Phys. Rev. D **73**, 014516 (2006). arXiv:hep-lat/0510074
41. F.E. Low, Phys. Rev. D **12**, 163 (1975)
42. S. Nussinov, Phys. Rev. Lett. **34**, 1286 (1975)
43. L.N. Lipatov, Sov. Phys. JETP **63**, 904 (1986)
44. Y.Y. Balitski, L.N. Lipatov, Yad. Fiz. **28**, 1597 (1978)
45. R. Brower, J. Polchinski, M. Strassler, C.-I. Tan, arXiv:hep-th/0603115
46. S. Erhan, P.E. Schlein, Eur. Phys. J. C **33**, 325 (2004)
47. S. Erhan, P.E. Schlein, Phys. Lett. B **481**, 177 (2000)
48. S. Erhan, P.E. Schlein, Phys. Lett. B **427**, 389 (1998)
49. A.B. Kaidalov, Yu.A. Simonov, Phys. Lett. B **477**, 163 (2000)
50. A.V. Dubin, A.B. Kaidalov, Yu.A. Simonov, Yad. Fiz. **63**, 1428 (2000)
51. J.D. Bjorken, E. Paschos, Phys. Rev. **185**, 1975 (1969)
52. A. Tang, J.W. Norbury, Phys. Rev. D **62**, 016006 (2000). arXiv:hep-ph/0004078
53. W.K. Tang, Phys. Rev. D **48**, 2019 (1993)
54. A. Brandt, S. Erhan, A. Kuzucu, D. Lynn, M. Medinnis, N. Ozdes, P.E. Schlein, M.T. Zeyrek, J.G. Zweizig, Nucl. Phys. B **514**, 3 (1998)
55. M.M. Brisudova, L. Burakovsky, T. Goldman, Phys. Rev. D **61**, 054013 (2000). arXiv:hep-ph/9906293
56. M.M. Brisudova, L. Burakovsky, T. Goldman, arXiv:hep-ph/9810296
57. M.M. Brisudova, L. Burakovsky, T. Goldman, A. Szczepaniak, Phys. Rev. D **67**, 094016 (2003). arXiv:nucl-th/0303012v2
58. G.S. Bali, Phys. Rep. **343**, 1–136 (2001). arXiv:hep-ph/0001312
59. N. Brambilla, A. Pineda, J. Soto, A. Vairo, Rev. Mod. Phys. **77**, 1423 (2005). arXiv:hep-ph/0410047
60. E. Eichten, S. Godfrey, H. Mahlke, J.L. Rosner, Rev. Mod. Phys. **80**, 1161 (2008). arXiv:hep-ph/0701208
61. E. Eichten, K. Gottfried, T. Kinoshita, K.D. Lane, T.-M. Yan, Phys. Rev. D **21**, 203 (1980)
62. C. Quigg, J.L. Rosner, Phys. Rep. **56**, 167–235 (1979)
63. M.N. Sergeenko, Z. Phys. C **64**, 315 (1994)
64. M.N. Sergeenko, Phys. At. Nucl. **56**, 365 (1993)
65. A. Kirk, Yad. Fiz. **62**, 439 (1999)
66. L. Morand et al. (The CLAS Collaboration), Eur. Phys. J. A **24**, 445–458 (2005). DAPNIA-05-54. JLAB-PHY-05-297. arXiv:hep-ex/0504057
67. L. Morand, D. Doré, M. Gar'con, M. Guidal, J.-M. Laget et al. (The CLAS collaboration), Phys. Rev. D **70**, 054023 (2004). arXiv:hep-ex/0504057v1
68. M. Battaglieri et al. (The CLAS Collaboration), Phys. Rev. Lett. **90**, 022002 (2003). JLAB-PHY-03-04. arXiv:hep-ex/0210023
69. M. Battaglieri et al. (The CLAS Collaboration), Phys. Rev. Lett. **87**, 172002 (2001). JLAB-PHY-01-104. arXiv:hep-ex/0107028
70. P.D.B. Collins, P.J. Kearney, Z. Phys. C **22**, 277 (1984)
71. M. Guidal, J.-M. Laget, M. Vanderhaeghen, Nucl. Phys. A **627**, 645 (1997)
72. J.-M. Laget, Phys. Rev. D **70**, 054023 (2004). JLAB-THY-04-67. DAPNIA-04-207. arXiv:hep-ph/0406153
73. F. Cano, J.M. Laget (DAPNIA, Saclay), Phys. Rev. D **65**, 074022 (2002). arXiv:hep-ph/0111146
74. S.J. Brodsky, G.R. Farrar, Phys. Rev. Lett. **31**, 1153 (1973)
75. M.N. Sergeenko, Phys. Rev. D **61**, 056010 (2000)
76. P.V. Landshoff, O. Nachtman, Z. Phys. C **35**, 405 (1987)
77. A.B. Kaidalov, Phys. Lett. B **116**, 459 (1982)
78. A.B. Kaidalov, K.A. Ter-Martirosyan, Phys. Lett. B **117**, 247 (1982)
79. G.I. Lykasov, G.H. Arakelian, M.N. Sergeenko, Phys. Part. Nucl. **30**, 343–368 (1999)
80. G.I. Lykasov, M.N. Sergeenko, Z. Phys. C **70**, 455 (1996)
81. G.I. Lykasov, M.N. Sergeenko, Z. Phys. C **56**, 697 (1992)
82. G.I. Lykasov, M.N. Sergeenko, Z. Phys. C **52**, 635 (1991)
83. P. González, V. Mathieu, V. Vento, arXiv:1108.2347v2
84. J. Sucher, Phys. Rev. D **51**, 5965 (1995)
85. C. Semay, R. Ceuleneer, Phys. Rev. D **48**, 4361 (1993)
86. M.N. Sergeenko, Mod. Phys. Lett. A **12**(37), 2859 (1997). arXiv:quant-ph/9911081v1
87. M.N. Sergeenko, Phys. Rev. A **53**, 3798 (1996). arXiv:quant-ph/9911075
88. M.N. Sergeenko, Mod. Phys. Lett. A **15**, 83 (2000). arXiv:quant-ph/9912069
89. M.N. Sergeenko, Mod. Phys. Lett. A **13**, 33 (1998). arXiv:quant-ph/9911089
90. M.N. Sergeenko, Int. J. Mod. Phys. A **18**, 1 (2003). arXiv:quant-ph/0010084
91. C. Semay, R. Ceuleneer, Phys. Rev. D **48**, 4361 (1992)
92. W.H. Blask et al., Z. Phys. A **337**, 327 (1990)
93. G.A. Baker, P. Graves-Morris, in *Padé Approximants*, ed. by G.-C. Rota (Addison-Wesley, London, 1981), pp. 287–305
94. K. Nakamura et al. (Particle Data Group), J. Phys. G **37**, 075021 (2010), and 2011 partial update for the 2012 edition
95. J.R. Cudell, A. Donnachie, P.V. Landshoff, Phys. Lett. B **448**, 281 (1999)